Analog-Computer Studies of Josephson Radiation Effects

N. R. WERTHAMER AND SIDNEY SHAPIRO*

Bell Telephone Laboratories, Murray Hill, New Jersey

(Received 17 July 1967)

Equations characterizing a Josephson junction coupled to a resonant cavity driven by an rf voltage have been programmed for an electronic analog computer. Modifications in the dc V-I characteristic of the junction, for both constant-voltage and constant-current load lines, as well as the power spectrum in the cavity, were observed as a function of the parameters: resonance frequency and Q of the cavity, frequency and amplitude of the applied rf voltage, and strength of coupling between junction and cavity. Many of the nonlinear, parametric effects observed can also be understood analytically on the basis of the approximation that the cavity electric field contains only a single frequency component.

I. INTRODUCTION

THE ac Josephson effect,[1–5] i.e., the existence of alternating currents between two superconductors separated by a barrier when a dc voltage is maintained between them, has been confirmed in a variety of ways. Experiments have been carried out in which radiation from these alternating currents has been directly observed,[6–10] in which these currents have been self-detected via their interaction with resonant modes of tunnel junctions,[11–17] and in which these currents have been detected via their interaction with externally applied radiation.[18,19] In each case the observations have emphasized the strongly nonlinear nature of the ac Josephson effect, and confirmed the presence of current at many discrete frequencies simultaneously. More recently, experiments have demonstrated harmonic generation from Josephson junctions[20] and nonlinear interactions of a paramagnetic type associated with the ac Josephson effect.[21,22]

The wealth of nonlinear phenomena, involving as they do the many physical parameters pertaining to the Josephson effect itself, the coupling to radiation fields, whether self-generated or applied, and the geometric configuration of the junction, whether self-resonant or not, makes analysis a formidable task. Although the problem can be precisely formulated,[23] solutions have been obtained only for certain cases and then only with somewhat restrictive approximations.[13,16,23–25] It is possible, however, as shown in Sec. II, to reduce the problem to a form that is readily handled on an analog computer, while retaining much of the physics and, in particular, the nonlinear coupling between the junction and the radiation fields. Furthermore, analog simulation of the pertinent equations permits nearly exact solutions to be displayed and studied with comparative ease for a wide range of parameters.

An advantage of the analog computer is that the relative importance of the many parameters involved is readily revealed for cases of physical interest. One consequence has been the discovery of an appropriate simplifying approximation which has made possible an extensive analytical treatment. The work as a whole has led to quantitative predictions, which are subject to experimental test, about the characteristics of a junction and its radiation.

* Present address: Department of Electrical Engineering, University of Rochester, Rochester, New York.

[1] B. D. Josephson, Phys. Letters **1**, 251 (1962).
[2] B. D. Josephson, Rev. Mod. Phys. **36**, 216 (1964).
[3] B. D. Josephson, Advan. Phys. **14**, 419 (1965).
[4] P. W. Anderson, in *Lectures on the Many-Body Problem*, edited by E. R. Cainaiello (Academic Press Inc., New York, 1964), Vol. 3.
[5] P. W. Anderson, in *Progress in Low Temperature Physics*, edited by C. J. Gorter (North-Holland Publishing Company, Amsterdam, 1967), Vol. 5.
[6] I. K. Yanson, V. M. Svistunov, and I. M. Dmitrenko, Zh. Eksperim. i Teor. Fiz. **48**, 976 (1965) [English transl.: Soviet Phys.—JETP **21**, 650 (1965)].
[7] I. M. Dmitrenko and I. K. Yanson, Zh. Eksperim. i Teor. Fiz. Pis'ma v Redaktsiyu **2**, 242 (1965) [English transl.: JETP Letters **2**, 154 (1965)].
[8] D. N. Langenberg, D. J. Scalapino, B. N. Taylor, and R. E. Eck, Phys. Rev. Letters **15**, 294 (1965); **15**, 842 (E) (1965).
[9] A. H. Dayem and C. C. Grimes, Appl. Phys. Letters **9**, 47 (1966).
[10] J. E. Zimmerman, J. A. Cowen, and A. H. Silver, Appl. Phys. Letters **9**, 353 (1966).
[11] R. E. Eck, D. J. Scalapino, and B. N. Taylor, Phys. Rev. Letters **13**, 15 (1964).
[12] M. D. Fiske, Rev. Mod. Phys. **36**, 221 (1964).
[13] R. E. Eck, D. J. Scalapino, and B. N. Taylor, in *Proceedings of the 9th International Conference on Low Temperature Physics*, edited by J. G. Daunt, D. V. Edwards, F. J. Milford, and M. Yaqub (Plenum Press, Inc., New York, 1965), p. 415.
[14] I. M. Dmitrenko, I. K. Yanson, and V. M. Svistunov, Zh. Eksperim. i Teor. Fiz. **49**, 1741 (1965) [English transl.: Soviet Phys.—JETP **22**, 1190 (1966)].
[15] C. B. Satterthwaite, M. G. Craford, R. N. Peacock, and R. F. Ries, in *Proceedings of the 9th International Conference on Low Temperature Physics*, edited by J. G. Daunt, D. V. Edwards, P. J. Milford, and M. Yaqub (Plenum Press, Inc., New York, 1965), p. 443.
[16] D. D. Coon and M. D. Fiske, Phys. Rev. **138**, A744 (1965).
[17] D. N. Langenberg, D. J. Scalapino, and B. N. Taylor, Proc. IEEE **54**, 560 (1966).
[18] S. Shapiro, Phys. Rev. Letters **11**, 80 (1963).
[19] S. Shapiro, A. R. Janus, and S. Holly, Rev. Mod. Phys. **36**, 223 (1964).
[20] S. Shapiro, J. Appl. Phys. **38**, 1879 (1967).
[21] A. H. Silver and J. E. Zimmerman, Appl. Phys. Letters **10**, 142 (1967).
[22] H. Zimmer, Appl. Phys. Letters **10**, 193 (1967).
[23] N. R. Werthamer, Phys. Rev. **147**, 255 (1966).
[24] I. O. Kulik, Zh. Eksperim. i Teor. Fiz. Pis'ma v Redaktsiyu **2**, 134 (1965) [English transl.: JETP Letters **2**, 84 (1965)].
[25] P. Lebwohl and M. J. Stephen (to be published).

In this paper, we report on our analog computations as well as the associated analytical work. The following Sec. II reviews the nonlinear equations describing the junction and discusses the physical approximations made in order to reduce these equations to a form suitable for the analog computer. Programming techniques are detailed in Sec. III, and limitations on the accuracy of the solution are discussed. The solutions themselves are presented in Sec. IV, and significant features are pointed out and discussed. Section V shows how a class of solutions generated by the computer may also be obtained by an analytical treatment based on an appropriate approximation. A summary of the paper forms the final Sec. VI.

II. REVIEW OF EQUATIONS FOR JUNCTION RADIATION

The natural mathematical starting point consists of Maxwell's equations for the electromagnetic fields generated by current sources, together with the constitutive relations for the current as a functional of the fields. Because the ac magnetic fields are unimportant for the constitutive relations,[23] we write the ac portion of Maxwell's equations in the form

$$\left(\nabla^2-\frac{1}{c^2}\frac{\partial^2}{\partial t^2}\right)\mathbf{E}(\mathbf{r},t)=\frac{4\pi}{c^2}\frac{\partial}{\partial t}\mathfrak{J}(\mathbf{r},t). \tag{1}$$

The static magnetic field staisfies

$$\nabla^2\mathbf{H}(\mathbf{r})=(4\pi/c)\,\nabla\times\langle\mathfrak{J}(\mathbf{r},t)\rangle_t, \tag{2}$$

where the $\langle\ \rangle_t$ denotes time average, and gaussian units are used, as will be true throughout this paper.

Since these equations are to be solved subject to boundary conditions, the geometrical configurations we are considering must be specified. We regard the tunneling current as flowing between two superconductors with plane parallel surfaces, i.e., separated by an insulator of uniform thickness. Each of the superconductors we take to be both thick and wide compared to a superconducting penetration depth, and to avoid unnecessary complication we take the two superconductors to be identical in composition. We also consider the junction (the two superconductors and their contact area) to be placed in a metallic enclosure.

The constitutive relations separate naturally into two parts, those for the metallic regions and those for the insulating barrier region. In the metals it suffices to assume a simple classical skin effect for the ac component and London's equation for the dc component,

$$(4\pi/c^2)\,(\partial/\partial t)\mathfrak{J}(\mathbf{r},t)=(1/\Lambda^2)\,\mathbf{E}(\mathbf{r},t), \tag{3}$$

$$(4\pi/c)\,\nabla\times\langle\mathfrak{J}(\mathbf{r},t)\rangle_t=-(1/\lambda^2)\mathbf{H}(\mathbf{r}), \tag{4}$$

with

$$\Lambda^{-2}=\lambda^{-2}+2i\delta^{-2}, \tag{5}$$

where λ is the penetration depth, and δ is the classical skin depth. In the insulating region, the tunneling current is given by

$$\mathfrak{J}(\mathbf{r},t)=\hat{n}\,\mathrm{Im}\int_{-\infty}^{t}dt'\{K_1(t-t')\,\exp(i/2)\times[\Phi(\mathbf{r},t)-\Phi(\mathbf{r},t')]+iK_2(t-t')\times\exp(i/2)[\Phi(\mathbf{r},t)+\Phi(\mathbf{r},t')]\}, \tag{6}$$

where $\hat{n}$ is the unit normal to the barrier plane. The kernels K_1 and K_2 are detailed in Ref. 23. The phase $\Phi(\mathbf{r},t)$ is related to the voltage difference between the two superconductors and to the static magnetic flux enclosed by the junction area,

$$\Phi(\mathbf{r},t)=\frac{2e}{\hbar}\int_{-\infty}^{\infty}d(\hat{n}\cdot\mathbf{r})\hat{n}\cdot\left[c^{-1}\mathbf{A}(\mathbf{r})+\int_{-\infty}^{t}dt'\mathbf{E}(\mathbf{r},t')\right]. \tag{7}$$

Here $\mathbf{A}(\mathbf{r})$ is the vector potential of the static magnetic field.

The solution of Maxwell's equations driven by the sources is a standard, although usually quite involved, mathematical problem The complete solutions must be obtained for the insulator, for the surrounding enclosure, and for the metals separately; then these solutions must be matched across the surfaces of discontinuity. This program has been carried out for several rather restricted special cases, but never for the most general situation. Nonetheless, some simple qualitative statements can be made. First, the combined volume of insulator, enclosure, and metals has a set of approximate normal modes, approximate in the sense that they are weakly damped by the metallic losses. The character of these modes, i.e., the distribution of fields in them, depends on the dimensions of the three regions relative to each other and to the wavelength of the radiation involved. The extent to which each of these modes is excited by the tunneling current depends on the spatial overlap of the field and current distributions. The current distribution, in turn, is affected by the relative strengths of the various excited normal-mode contributions to the voltage. The current distribution is also modified by the net static magnetic field.

Furthermore, the nonlinearity of the constitutive relation introduces coupling between all normal modes. Although it is likely (from study of mode competition in lasers) that only a single mode will be dominantly excited at any one moment, it is possible for one mode to excite another with substantial transfer of energy between the two, depending on the strength of the nonlinearity. An added complication is the static magnetic field, which is also coupled to the ac modes and whose external variation can "steer" the current from one to another mode.

The full problem is thus both intricately rich in physical variety and well beyond the capacity of an analog computer. Since both partial differential equations and integro-differential equations are extremely

difficult to solve on an analog computer, we are forced to make alterations in both the spatial degrees of freedom and the integral kernels of Eq. (6).

Turning first to the kernels, the fact that they are retarded reflects the voltage dependence of the current amplitudes. Such a dependence is of course well known for single-particle tunneling (the term containing K_1), where the current rises sharply toward the normal resistive characteristic as the voltage is increased past 2Δ. For pair tunneling (the term containing K_2) the dependence was not mentioned by Josephson[1] and is even now not widely appreciated. These retardation, or voltage-dependent, effects only appear for voltages and frequencies in the neighborhood of 2Δ;[23,26] if attention is restricted to frequencies low compared to 2Δ, we may make the approximations

$$K_1(t-t')\cong K_2(t-t')\cong j_J\delta(t-t'), \tag{8}$$

so that

$$\mathfrak{J}(t)\cong j_J\cos\Phi(t). \tag{9}$$

The tunneling current amplitude is given by

$$j_J=\pi\Delta/2eR, \tag{10}$$

where R is the normal resistivity of the junction. A related but more convenient quantity is the "Josephson plasma frequency" ω_J, defined as[27]

$$\omega_J^2\equiv 2ej_J/\hbar C=\pi\Delta/\hbar RC, \tag{11}$$

where C is the junction capacitance per unit area.

The spatial degrees of freedom in Eqs. (3) and (4) must also be altered. Nevertheless, the time-dependent problem that remains intact still contains most of the interesting physics of the Josephson effect. The alterations we make are motivated from the results previously obtained[23] in the particular case of a wide junction, for which traveling-wave rather than standing-wave boundary conditions could be used. Along with the traveling-wave hypothesis, it was also assumed there that the junction was in a static magnetic field which was everywhere uniform, meaning that the self-field limiting of a wide junction[28,29] was ignored. With these assumptions, the partial differential equations reduce to ordinary differential equations in the phase variable

$$\varphi=\Omega_{dc}t-\kappa_{dc}z, \tag{12}$$

where Ω_{dc} is proportional to the applied dc voltage, $\Omega_{dc}=2eV_{dc}/\hbar$, and κ_{dc} is proportional to the applied dc magnetic field. The Maxwell's equations can then be solved exactly in terms of the current sources; the boundary conditions can be matched at the insulator-superconductor interfaces; and the electric field can be eliminated in favor of the ac voltage across the junction. The results of this analysis are that the current density can be expressed as

$$\mathfrak{J}=\mathfrak{J}(\Phi(\varphi)),$$

where Φ equals φ plus the additional phase induced by the self-coupling through the metal, and that the Fourier transform of $\Phi(\varphi)-\varphi$ is linearly related to that of $\mathfrak{J}(\varphi)$:

$$\mathfrak{J}(\varphi)=\int_{-\infty}^{\infty}d\mu\,\exp(i\mu\varphi)\mathfrak{J}_\mu, \tag{13}$$

$$\Phi(\varphi)-\varphi=\int_{-\infty}^{\infty}d\mu\,\exp(i\mu\varphi)\,R_\mu\mathfrak{J}_\mu, \tag{14}$$

$$R_\mu=(4\pi/\mu^2)(2e/\hbar C)[\Omega_{dc}^2-(c\kappa_{dc})^2/2\Lambda_\mu C]^{-1}. \tag{15}$$

Using Eq. (5) in the limit of penetration depth much shorter than skin depth, $\lambda\ll\delta$, we obtain

$$\mathrm{Re}\Lambda_\mu^{-1}\cong\lambda^{-1}, \tag{16}$$

$$\mathrm{Im}\Lambda_\mu^{-1}\cong\lambda/\delta_\mu^2=2\pi\lambda\mu\Omega_{dc}\sigma/c^2, \tag{17}$$

where σ is the normal-metal dc conductivity.

Although these formulas are developed for traveling waves, the case of standing waves in narrower junctions is more relevant for most experimental situtations. However, standing waves introduce an intrinsic spatial dependence which we are here trying to avoid. We thus simulate the presence of a single standing wave by making the replacement

$$(\mu c\kappa_{dc})^2/2\lambda C\rightarrow\omega_c^2 \tag{18}$$

in Eqs. (15) and (16), where ω_c is now a phenomenological resonance frequency, and the corresponding replacement of the damping term,

$$i(\mu c\kappa_{dc})^2\lambda/2\delta_\mu^2C\rightarrow i\omega_c^2(\lambda/\delta_\mu)^2=i\mu\Omega_{dc}\gamma. \tag{19}$$

We introduce the frequency-independent loss factor

$$\gamma\equiv\omega_c(\lambda/\delta_c)^2,$$

where δ_c represents the skin depth at frequency ω_c. Thus

$$R_\mu\rightarrow 4\pi(2e/\hbar C)[(\mu\Omega_{dc})^2-\omega_c^2-i\mu\Omega_{dc}\gamma]^{-1}. \tag{20}$$

We now ignore static magnetic fields altogether. Furthermore, we assume that the effect of a surrounding metallic enclosure can be approximated by altering the values of ω_c and γ in Eq. (20), while leaving the functional form invariant.

When these replacements are made, the resulting Eqs. (9), (13), (14), and (20) become entirely equivalent to the differential equation

$$\left(\frac{d^2}{dt^2}+\gamma\frac{d}{dt}+\omega_c^2\right)\Omega(t)=\omega_J^2\frac{d}{dt}\cos\Phi(t), \tag{21}$$

using definition (11), together with

$$d\Phi(t)/dt=\Omega(t)+\Omega_{dc}. \tag{22a}$$

With the added possibility of an alternating applied

[26] E. Riedel, Z. Naturforsch. **19a**, 1634 (1964).
[27] B. D. Josephson, in *Quantum Fluids*, edited by D. F. Brewer (North-Holland Publishing Company, Amsterdam, 1966), p. 174.
[28] R. A. Ferrell and R. E. Prange, Phys. Rev. Letters **10**, 479 (1963).
[29] J. M. Rowell, Phys. Rev. Letters **11**, 200 (1963).

voltage to simulate the effect of an applied rf field,

$$d\Phi(t)/dt=\Omega(t)+\Omega_{dc}+\Omega_{rf}\cos\omega_{rf}t. \quad (22b)$$

Equations (21) and (22b) are the equations which we have programmed for the analog computer. [The phases of the current and the rf voltage have been fixed by the arbitrary but simple choice of $\Phi(0)=0$. This means that the zero-voltage Josephson current is a maximum.]

These equations, however, represent the junction in the so-called constant-voltage mode. That is, we have assumed that the external dc voltage source biasing the junction has a negligible series resistance. In practice, however, the series resistance is much larger than the resistance of the junction (unless an especial effort is made), so that the external source is actually a constant *current* source. In this case, Eq. (22b) is modified to

$$d\Phi(t)/dt=\Omega(t)+(\Omega_{dc}-\tfrac{1}{10}\langle\cos\Phi\rangle_t)+\Omega_{rf}\cos\omega_{rf}t, \quad (23)$$

while Eq. (21) remains the same. The factor $\frac{1}{10}$ is a convenient choice for amplitude scaling. The interpretation of Ω_{dc} is now that it is proportional to the direct *current* flowing through the junction, while $\Omega_{dc}-\frac{1}{10}\langle\cos\Phi\rangle_t$ is the resulting dc voltage. Equation (23) also implies that a parallel shunt resistor exists across the junction. This shunt simulates the single-particle tunneling current actually present in the junction, and must be taken into account here in order to prevent gross instability when the dc current is driven in excess of the maximum Josephson value.

III. PROGRAMMING FOR ANALOG COMPUTATION

Equations (21), (22b), and (23) were simulated on a commercial electronic analog computer (the Electronics Associates, Inc., model PACE TR48). This method of solution offers several advantages over the more usual digital computer procedures. First, since the nonlinearity involves only a simple trigonometric function, it is easily patched on the analog. In addition, the equations contain six adjustable parameters, all of which have physical significance. Since a solution is available on the analog within a fraction of a second for fixed values of these parameters, and since the parameters can be varied continuously and directly merely by turning potentiometer dials, the solutions can be quickly and conveniently mapped out in the six-parameter space. A further advantage for rapidly grasping the physical content of the solutions is that any intermediate variable in the program can be examined in detail at any desired time. The penalty that is paid for this convenience is a certain amount of inaccuracy and a limited capacity for mathematical complexity. For example, Eq. (6) far exceeds the capabilities of an analog of this type. Yet the TR48 possesses sufficient capacity to handle most cases of interest. Forty-eight operational amplifiers grouped so as to provide five quarter-square multipliers and 16 integrators provided us with a high degree of flexibility.

In general, the method employed in our work was to run the computer in the so-called "repetitive operation" (ro) mode. In this mode, after the computation proceeds for a time selected by the operator, initial conditions are automatically reset by machine control circuits and the computation is repeated. The full time-dependent solution, or, in fact, any variable represented by an accessible voltage in the machine, is displayed on an oscilloscope whose time sweep is synchronized internally to the selected computation time. When desired, a time-average value was obtained by filtering procedures, which will be described shortly, and the resulting solution was plotted on an X-Y recorder as a function of an appropriate variable.

The computation time, or time of solution, must be carefully adjusted to minimize solution error. On the one hand, too short a time of solution will not allow initial transients to die away sufficiently and thereby introduce errors in the desired steady-state solution. On the other hand, too long a time of solution also leads to inaccuracies, since integrator error increases with integrating time as a result of finite operational amplifier gain. After some experimentation a computation time of 200 msec was selected for our problem on the TR48 and virtually all subsequent work used that value. With this value the computation lasted for about a thousand integrator time constants before resetting and a good steady-state solution was obtained.

A minor inconvenience in plotting results on the X-Y recorder was occasioned by our choice of 200 msec for the computation time. Every time the machine reset itself a strong transient was introduced. Despite the filtering circuits through which the recorder was connected to the computer, these reset transients were sufficiently strong and at a sufficiently slow rate to cause the recorder pen to jump slightly. The resulting "jitter" in the recorder traces (visible, e.g., in Fig. 6) although annoying, was fortunately not severe. Thus it was decided to tolerate it rather than introduce further filtering to eliminate it, since additional filtering would have meant spending a prohibitively long time in plotting the data.

In addition to the choice of computation time, solution accuracy is also affected by the choice of scaling. The frequencies that appear in the physical problem must be scaled down so as to fall within that range where the operational amplifiers have an essentially flat frequency response. Care in frequency scaling is especially important for the Josephson problem since the strong nonlinearity means that the solutions are rich in harmonics. To minimize errors, the scaled frequencies corresponding to harmonics that have appreciable amplitude must also fall on the nearly flat portion of the amplifier frequency response. Despite our best efforts some errors resulting from

amplifier phase shift and from cross talk due to parasitic capacitance were unavoidable. In addition to frequency scaling, amplitude scaling is of importance. The dynamic range of the transistor amplifier used in the TR48 is, nominally, ±10 V and so care was taken that at no instant did any voltage in the problem exceed this range. The machine is equipped with warning lights that indicate an overload condition and help the operator prevent errors from poor amplitude scaling.

In general, accuracy of the order of 10% was obtained in those cases where the analog solution could be compared with an analytical solution. (see Sec. IV, case A). When a case was attempted where accuracy of at least 20% could not be attained because of a combination of the factors discussed above, no solution was recorded. With some experience in operating the TR48, and taking full advantage of the ability to observe any machine voltage as a function of time on the oscilloscope, the operator could readily identify such cases.

The patching diagram for the computation is shown in Fig. 1, using standard symbol conventions. (See

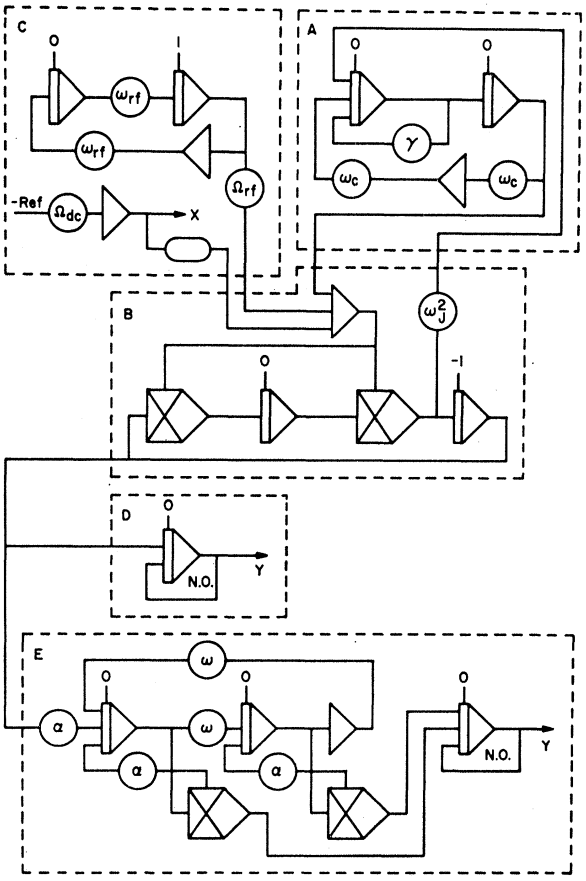

FIG. 1. Patching diagram for analog simulation of Eqs. (21), (22b), and (23).

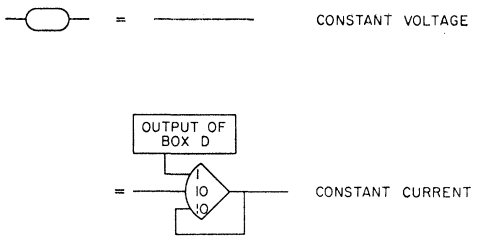

FIG. 2. Definition of symbol used in Fig. 1, indicating difference in patching between constant-voltage and constant-current dc circuits.

for example, Korn and Korn.[30]) The diagram is divided by dashed lines into blocks representing the analogs of various physical components. Block A corresponds to the electromagnetic resonator; block B represents the Josephson junction; block C is the analog of the external circuitry, supplying the dc voltage (or current) and the rf voltage modulation. The least obvious parts of the diagram are blocks D and E, which act as narrow-band filters by making use of a particular design feature of the analog machine. While the computer is running in the ro mode, a small portion of the machine can simultaneously be held in continuous, nonrepetitive operation at a rate 5000 times slower. We have used this latter portion (indicated in the diagram by the notation N.O.) as a dc filter, with output traced directly on an X-Y recorder versus some slowly and manually varied parameter. Block D produces $\langle \cos\Phi \rangle_t$, proportional to the dc component of the tunneling current, while block E produces the spectral power density at variable frequency ω and with frequency passband $\alpha \ll \omega$. That is, if the input to block E has the Fourier spectral representation

$$\cos\Phi(t) = (2\pi)^{-1} \int_{-\infty}^{\infty} d\omega f(\omega) \exp(i\omega t),$$

then the output from the block is approximately proportional to $|f(\omega)|^2$, provided that α is chosen much less than any other characteristic frequency in the equations.

Figure 1 has been drawn to represent both the constant voltage and constant current situations, the ambiguity being in the definition of the small oval in box C. The oval is shown in Fig. 2 to be merely a straight connection for the constant-voltage circuit, whereas in the constant-current case the more complicated circuit containing an added operational amplifier is necessary to represent Eq. (23).

Although Fig. 1 represents the patching of the problem constituted by Eqs. (21), (22b), and (23) in the form most often used, it is not the only possible patching nor necessarily the simplest. We make no attempt here to explain the patching in detail, and so we have even omitted indicating in Fig. 1 which of the quan-

[30] G. A. Korn and T. M. Korn, *Electronic Analog and Hybrid Computers* (McGraw-Hill Book Company, Inc., New York, 1964).

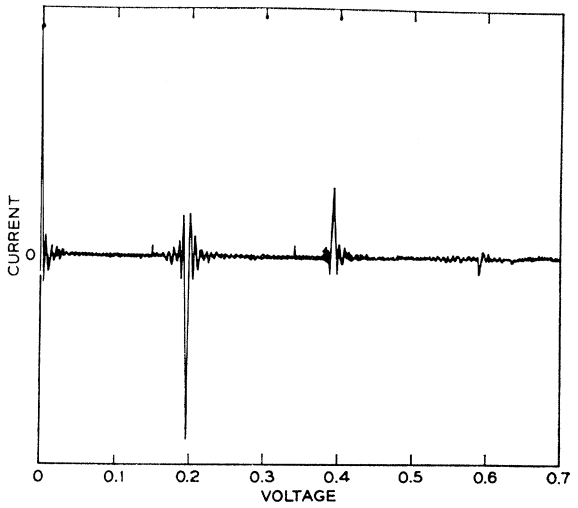

FIG. 3. Trace of the dc characteristic of junction, with rf voltage drive ($\omega_{rf}=0.2$) but no resonant cavity ($\omega_J=0$). Voltage units are arbitrary.

tities in Eqs. (21), (22b), and (23) are simulated by the various amplifier inputs. Any attempt to do so would needlessly lengthen this paper and elevate our particular patching to a position of uniqueness it does not merit.

IV. RESULTS OF ANALOG COMPUTATION

The equations in which we are interested contain six independent parameters, posing the problem of how best to present the solution as a function of this six-parameter family. We have here selected cases of most physical interest, representative of typical experimental conditions. We usually plot a dc characteristic for the junction; that is, the dc current drawn from the external circuit (relative to the maximum Josephson current j_J) versus the dc bias voltage. This type of plot not only is the standard one experimentally, but also indicates clearly the amount of power supplied by the dc battery and converted into ac, available either in the rf driving field or in the electromagnetic resonator.

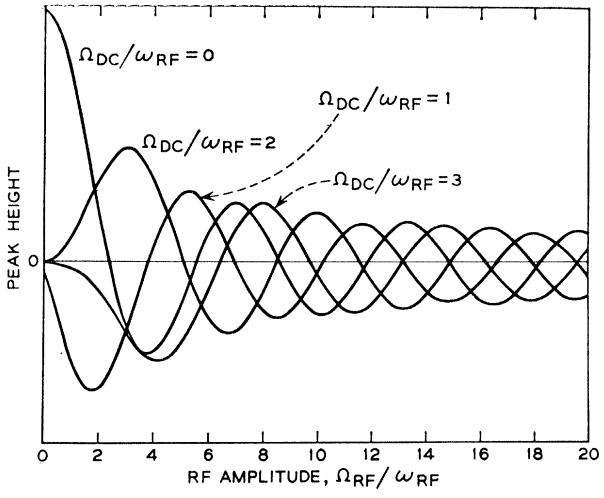

FIG. 4. Heights of the peaks in Fig. 3 as a function of normalized rf amplitude Ω_{rf}/ω_{rf}.

A. Applied rf Voltage without Resonant Cavity

The first and simplest situation we consider is the junction driven by an rf voltage but without any feedback via the resonant cavity ($\omega_J=0$). It is well known that this produces simple frequency modulation of the Josephson current[19]; the dc characteristic should analytically be a sum of delta functions with Bessel-functions coefficients:

$$\langle \cos\Phi \rangle_t = \sum_{n=0}^{\infty} (-1)^n J_n\left(\frac{\Omega_{rf}}{\omega_{rf}}\right)\delta(\Omega_{dc}-n\omega_{rf})/\delta(0). \quad (24)$$

Figure 3 shows the dc characteristic produced by the analog, for rf frequency $\omega_{rf}=0.2$ and rf amplitude $\Omega_{rf}=0.25$. The curve serves primarily to illustrate the degree of accuracy that can be expected from the analog machine. Although the spikes predicted from Eq. (24) do appear at very nearly the correct position, corresponding to $n=0$, 1, 2, and 3, the finite frequency bandwidth of the operational amplifiers introduces the added oscillations seen adjacent to the main peaks. The flat portions of the curve show some of the "jitter" mentioned early in the previous section.

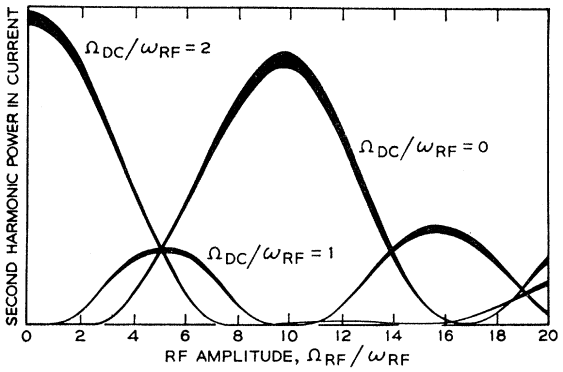

FIG. 5. Spectral power (arbitrary units) of the Josephson current, at the second harmonic of the rf frequency, when biased to a peak in the dc characteristic.

The amplitude of the main peaks are also nearly correct. Figure 4 shows the height of several of these peaks as a function of the normalized rf amplitude Ω_{rf}/ω_{rf}. These curves conform to within 10% of the functions $(-1)^n J_n(\Omega_{rf}/\omega_{rf})$ expected from Eq. (24). (The curves were obtained by driving the X axis of the X-Y recorder with a voltage proportional to Ω_{rf}, at fixed Ω_{dc}.) The accuracy is limited by the fact that the positions of the peaks drift slightly with respect to Ω_{dc}, a shift which is difficult to compensate for.

In addition to the dc characteristic, the spectral

power in the Josephson current at the second harmonic of the rf frequency was also obtained.[20] Figure 5 shows the output of the spectral power analyzer, box E in Fig. 1, when the dc bias is at an integral multiple of the rf frequency. The analyzer is set at $\omega=2\omega_{rf}$ and $\alpha=\omega/100$. The output is in arbitrary units, but is expected to be proportional to the function

$$J_{2-n}^2(\Omega_{rf}/\omega_{rf})+J_{2+n}^2(\Omega_{rf}/\omega_{rf})+(-1)^{n+1}2J_{2-n}(\Omega_{rf}/\omega_{rf}) \times J_{2+n}(\Omega_{rf}/\omega_{rf})\cos 2(\varphi_0-n\theta).$$

The initial phase of the Josephson current, φ_0, and the phase of the applied rf, θ, are set in our problem at the values $\pi/2$ and 0, respectively; but in an experiment φ_0 and $\varphi_0-n\theta$ would adjust as required by any applied magnetic field, by the current driven through the junction and by Maxwell's equations. The actual accuracy is only about 15–20% and there is substantially greater distortion at low output levels. Thus the spectral analyzer circuit is satisfactory in a qualitative way, but is not good for quantitative detail.

B. Resonant Cavity without Applied rf Voltage

With the capabilities and limitations of the analog machine spelled out by comparison in the above situation with solutions known analytically, we turn to a more interesting situation where analysis has not previously been available. We consider the junction coupled to the resonant electromagnetic cavity ($\omega_J\neq 0$) without any applied rf voltage ($\Omega_{rf}=0$), and plot the dc characteristic for various coupling strengths ω_J. This appears in Fig. 6, where the current axis is in arbitrary units with zero displaced for each curve. For clarity in the figure, the low-voltage regions are not shown. The cavity resonant frequency ω_c has been chosen equal to 0.2, and the damping constant γ is such that the cavity "Q" is $Q=\omega_c/\gamma=7.5$. Although desirable to sharpen detail, significantly higher Q values tend to introduce amplifier overload and could not be used. It is important to recognize that the dc current is nonvanishing (and hence nontrivial) only because the cavity damping is different from zero. To repeat a point made earlier, the dc characteristic is a measure of the power being supplied from the external battery into the electromagnetic radiation, and hence is a measure of the power which can be radiated by the junction.

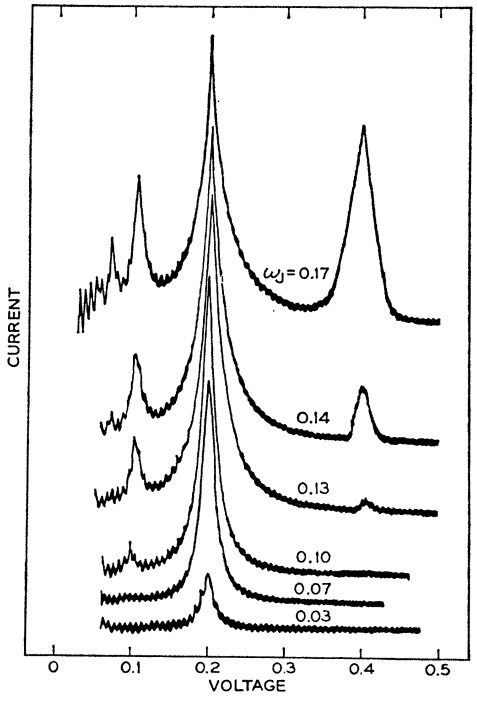

FIG. 6. The dc characteristic of the junction coupled to a resonant electromagnetic cavity ($\omega_c=0.2$, $\omega_c/\gamma=7.5$), for various coupling strengths ω_J, without applied rf voltage ($\Omega_{rf}=0$). The current axis is in arbitrary units, with zero displaced for each curve. The right-hand asymptote is very nearly the zero of current. The voltage units are also arbitrary.

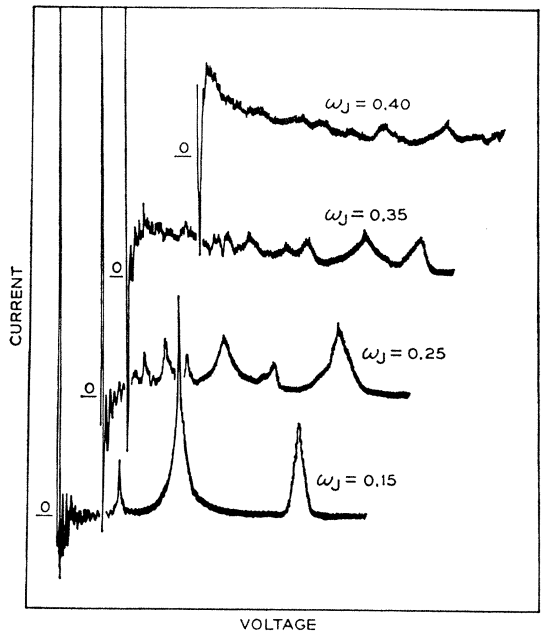

FIG. 7. The dc characteristic as in Fig. 6, but for substantially larger values of ω_J. Both current and voltage scales are displaced for each curve.

Several features in Fig. 6 are worth attention. First, a fundamental absorption peak occurs centered at $\Omega_{dc}=\omega_c$. Contrary to some earlier statements in the literature,[31] the center of the peak does not shift in frequency with changing ω_J. At low ω_J (e.g., $\omega_J\sim 0.03$), this is the only structure in the curve, and the peak is reminiscent of a Lorentzian line. As ω_J is increased (up to $\omega_J\sim 0.13$), the peak grows rapidly in height, broadens somewhat and distorts from the Lorentzian shape by becoming cusplike near the center. Further increases in ω_J, up to ~ 0.17, produce a diminishing increase in peak height and width, but a distinct sharpening of the central cusp.

[31] E. E. H. Shin and B. B. Schwartz, Phys. Rev. 152, 207 (1966).

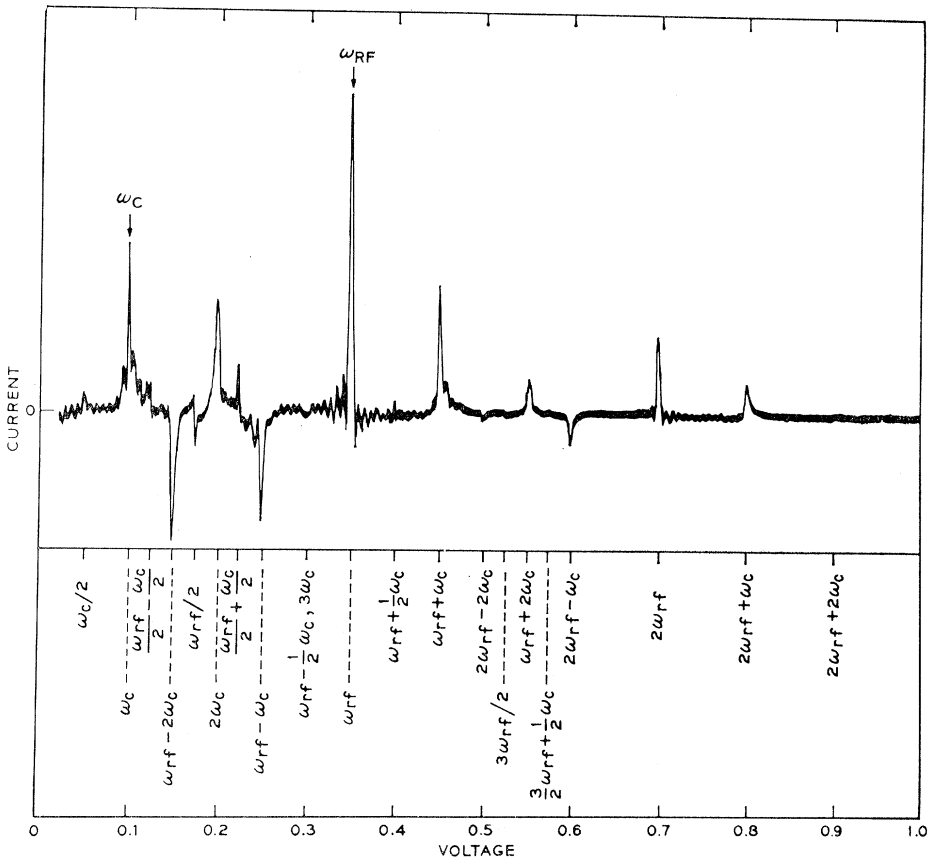

FIG. 8. The dc characteristic of the junction, both coupled to a resonant electromagnetic cavity ($\omega_c = 0.1$, $\omega_c/\gamma = 10.0$, $\omega_J = 0.063$) and driven by an rf voltage ($\omega_{rf} = \Omega_{rf} = 0.35$). Voltage units are arbitrary.

Another feature is the presence of a smaller absorption peak at the first subharmonic of the cavity frequency, $\Omega_{dc} = \omega_c/2$, which grows continuously with increasing ω_J and displays roughly the same changes in shape as the fundamental peak. At $\omega_J = 0.17$, the next subharmonic, $\Omega_{dc} = \omega_c/3$, is also clearly observable.

Finally, and in some respects most strikingly, an absorption peak appears at the second harmonic, $\Omega_{dc} = 2\omega_c$. However, this peak does not occur until a finite threshold in ω_J is reached (just under 0.13), whereupon it grows very rapidly in height and width with only small further increases in ω_J. This second harmonic peak is very close in shape to a straight-sided triangle and, as is seen most clearly in the curve $\omega_J = 0.14$, joins the background at a sharp corner rather than with a long sloping tail, as does the fundamental peak.

The dc characteristic for substantially larger ω_J is shown in Fig. 7. Here, for clarity, both the current and voltage scales are displaced for each curve, because the low-voltage region is now drawn in. Drastic changes in the characteristic take place as ω_J is increased from 0.15 to 0.40. The few well-defined absorption peaks present for $\omega_J = 0.15$ *decrease* in height and broaden substantially. Also, they are joined by many other peaks, such as at $\Omega_{dc} = 3\omega_c/2$ and at $\Omega_{dc} = \omega_c/n$ for quite a few integers n. As the peaks overlap each other for large ω_J, the characteristic smooths out on a broad scale, but shows a very complicated fine structure. The most important feature is that the current shoots up as the voltage is increased slightly from zero, and then very gradually decreases with further increase of voltage. This behavior is reminiscent of the large "excess currents" observed experimentally in point-contact junctions, where the coupling of current to radiation is believed to be strong.[20,32] The effect is due physically to the large number of subharmonics of ω_c in the ac-current frequency spectrum which can radiate into the cavity because of the strong nonlinearity.

Steps in current resulting from the coupling of a Josephson junction to modes of an external resonant cavity have been reported by Dayem and Grimes[9]; similar steps associated with self-resonances of a junction have been reported by a number of authors.[11–17] In all these cases the observations correspond only to the fundamental peak in the spectrum as shown in Fig. 6; the remaining lines await observation.

Study of the analog solution showed that, on each of the lines shown in Figs. 6 and 7, the cavity voltage wave form contained essentially only a single frequency equal to the cavity resonant frequency. This obser-

[32] J. E. Zimmerman and A. H. Silver, Phys. Rev. **141**, 367 (1966).

vation formed the basis for the analytical work reported in Sec. V.

C. Resonant Cavity together with Applied rf Voltage

Figure 8 shows the dc characteristic for a junction, both coupled to a resonant electromagnetic cavity and driven by an applied rf voltage. The cavity is chosen with $\omega_c=0.1$ and $Q=\omega_c/\gamma=10.0$, while the rf voltage has frequency $\omega_{rf}=0.35$ and amplitude $\Omega_{rf}=0.35$. The coupling of junction to cavity is $\omega_J=0.063$. This particular set of parameters is selected so as to give clear, well-developed nonlinear effects in both the radiative self-coupling and the rf frequency-modulation situations separately, and to give a good balance of the two effects relative to each other. The dc characteristic contains a wealth of structure, whose positions we have identified with sums and differences of multiples and submultiples of the cavity and rf frequencies. (One or two of the weakest lines, which are virtually imperceptible in the figure, appear with more definition in the original recorder tracing.)

Such a dc characteristic is closely related to the recent experiment of Silver and Zimmerman,[21] where a point contact junction was used to detect the Co^{59} nuclear resonance in a nearby sample. In their experiment the junction was driven weakly by an rf voltage source, and the frequency component of the ac current at ω_{rf} was measured, thus yielding a curve approximating the first derivative of the dc characteristic.

The lines in Fig. 8 fall into several series. The lines labeled ω_{rf} and $2\omega_{rf}$ arises solely from the presence of the applied rf and are similar to those shown in Fig. 3. The lines labeled $\omega_c/2$, ω_c and $2\omega_c$ arise solely from the coupling of the junction to the resonant cavity and are similar to those shown in Fig. 6. The remaining lines result from the parametric interaction of the

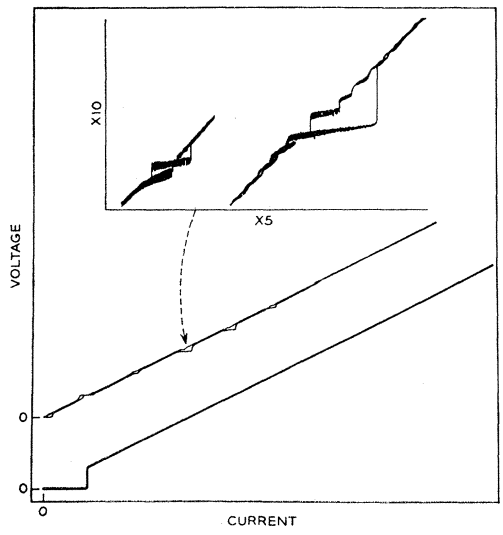

FIG. 9. The characteristics of the junction with constant-current external circuit, with and without applied rf voltage.

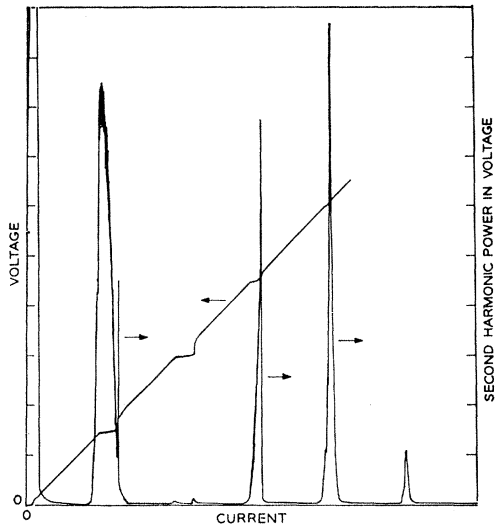

FIG. 10. The dc characteristic and spectral power of voltage at twice the applied rf frequency, of the junction with constant-current external circuit and with applied rf voltage.

applied rf, the resonant cavity, and the Josephson ac determined by the bias voltage. The lines labeled $\omega_{rf}+\frac{1}{2}\omega_c$, $\omega_{rf}+\omega_c$, $\omega_{rf}+2\omega_c$, $2\omega_{rf}+\omega_c$, and $2\omega_{rf}+2\omega_c$ are absorptive in character. For these lines the cavity serves as idler, the Josephson ac as pump, and the applied rf as signal in the usual parametric amplifier terminology. The lines labeled $\omega_{rf}-2\omega_c$, $\omega_{rf}-\omega_c$, $\omega_{rf}-\frac{1}{2}\omega_c$, $2\omega_{rf}-2\omega_c$, and $2\omega_{rf}-\omega_c$ are emissive in character. The cavity is again the idler but now the applied rf is the pump and the Josephson ac is the amplified signal. Therefore, since less current is needed from the dc bias circuitry to maintain the junction voltage, the current falls which, in the analog, corresponds to a negative current. Finally there remain the lines involving half-integral values of the rf. They are dispersive in character and although they represent one of the more striking effects of the nonlinear interaction between junction, cavity, and rf, they are not readily understood in terms of parametric amplification since the cavity is not driven on resonance.

The positions and shapes of lines such as are shown in Fig. 8 are taken up in the analytical work of Sec. V, under the approximation mentioned at the end of Sec. IVB that the cavity contains essentially a single frequency.

D. Constant-Current dc Circuit

The results presented so far have all been with a constant-voltage circuit. Results for the dc characteristic with a constant-current circuit are shown in Figs. 9 and 10. No resonant-cavity coupling is introduced ($\omega_J=0$). In Fig. 9 the lowest curve is the dc characteristic in the absence of applied rf voltage, showing a zero-voltage Josephson current and a switching transient to a normal shunt resistance. The curve above it (with shifted origin), is similar but with a substan-

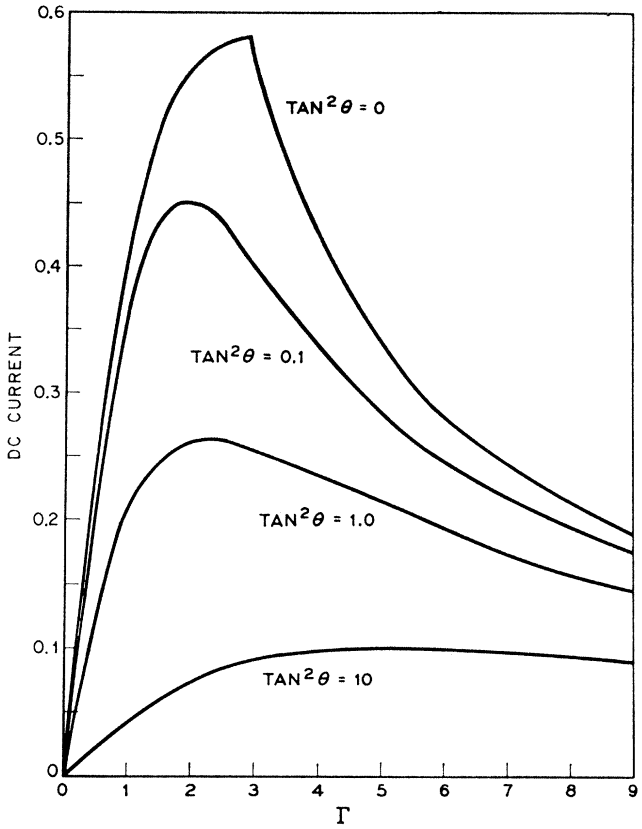

FIG. 11. The dc component of current versus Γ, for various tanθ; $m=1$.

tial applied rf voltage. Steplike breaks in the characteristic at dc voltage multiples of the rf frequency are clearly observed. The curve was traced by running the current from zero up to its maximum value and then down to zero again as indicated by the hysteresis in the step regions. The inset at the top of Fig. 9 shows one of the steps on an expanded scale. Two curves differing only in computation time are shown. The differences are pronounced and serve to illustrate the difficulty in working in the constant-current mode. How long the solution remains on a constant-voltage step and how soon the solution falls onto such a step depends on a number of factors: how near the current is to the maximum for the step, how slowly the current is swept, and how severe are machine transients and fluctuations. The additional steplike structure visible in the right-hand curve is a consequence of frequency scaling. As in a real junction, the frequency of the Josephson ac in the analog is proportional to the dc voltage; however, because of frequency scaling, the Josephson frequency is in the range of tens of cycles. The beating between the Josephson ac and the applied rf in the analog produces frequencies which are near to, but not equal to, zero whenever the voltage is near to, but not on, a constant-voltage step. Whenever such a difference frequency is equal to the machine repetition rate or to a multiple of that rate, the resulting synchronism leads to a tendency for the solution to lock-in over a range of current. This manifests itself via the additional steps in the V-I curve. Such steplike regions are also present in the left-hand curve of the inset but are not readily visible because the slower repetition rate causes them to be much closer together in voltage and thereby to be obscured by the ever-present solution noise and recorder pen "jitter."

Except for these steplike regions, which are a concomitant of unavoidable frequency scaling in the problem, the instability problems encountered on the analog computer in the constant-current mode are also encountered in experiments employing essentially constant-current circuitry. Thus our results serve to emphasize the care with which one must interpret such experiments, particularly when making use of data on the maximum amplitude of Josephson current, whether at zero voltage or in a constant-voltage step. The limited usefulness of the analog technique in the constant-current mode discouraged us from investigating in that mode more interesting cases, such as those involving a cavity.

One additional case, however, was studied in the constant-current mode and the results are presented in Fig. 10. The dc V-I characteristic is plotted in the presence of some rf power at $\omega_{rf}=0.15$ and, on the same current scale, the corresponding second harmonic power in voltage, i.e., with the analyzer set at a frequency of 0.3. In each case the current was swept only

in one direction, from zero to some maximum positive value. These results show the extremely complex harmonic generation patterns encountered with Josephson junctions and can be compared with recent experiments on this property.[20] Note in the figure that in addition to the harmonic power associated with the Josephson effect, the transient associated with switching off of a step also generates harmonics.

V. APPROXIMATE ANALYTICAL TREATMENT

Use of the analog computer for studying Eqs. (21) and (22b) has also enabled us to realize that there exists for them a valid and useful physical approximation. In examining during the simulation the ac voltage $\Omega(t)$ in the resonant cavity, we found that whenever a significant amount of power was being drawn from the dc battery and into the cavity, the predominant frequency component of $\Omega(t)$ was the cavity resonant frequency, even though the Josephson frequency Ω_{dc} had a different value. This suggested to us the approximation that only a single frequency component close to ω_c be allowed for the $\Omega(t)$ appearing in the constitutive relation. The approximation then reduces the nonlinear differential equation to an implicit algebraic equation which can be treated in detail.

More precisely, we return to the differential equation

$$\left(\frac{d^2}{dt^2}+\gamma\frac{d}{dt}+\omega_c^2\right)\Omega(t)=\omega_J^2\frac{d}{dt}\cos\left(\Omega_{dc}t+\int^t dt'\Omega(t')\right), \quad (25)$$

and we assume that the dc voltage bias is near to an integer multiple of ω_c:

$$\omega\equiv\Omega_{dc}/m\approx\omega_c, \qquad m=\text{integer}. \quad (26)$$

The approximation is to consider only the single frequency component of $\Omega(t)$ at ω,

$$\int^t dt'\Omega(t')\cong Z\cos(\omega t+\varphi), \quad (27)$$

where only the amplitude Z and phase shift φ are to be determined. Equation (25) then reduces to

$$Z=-2i\Gamma\cos\theta\exp(-i\theta)(2\pi)^{-1}$$
$$\times\int_0^{2\pi} d(\omega t)\exp[-i(\omega t+\varphi)]\cos(m\omega t+Z\cos(\omega t+\varphi))$$
$$=i\Gamma\cos\theta\exp(-i\theta)\{\exp[-im(\varphi+\pi/2)]J_{m-1}(Z)$$
$$+\exp[im(\varphi+\pi/2)]J_{m+1}(Z)\}. \quad (28)$$

Again, the J's are Bessel functions. We have also introduced the definition

$$\omega_J^2/(\omega_c^2-\omega^2+i\gamma\omega)\equiv-i\Gamma\cos\theta\exp(-i\theta), \quad (29)$$

where Γ and θ are real. It is convenient to assume a narrow resonance, so as to make the replacement $\gamma\omega\to\gamma\omega_c$ in Eq. (29) Then inverting the relation,

$$\Gamma=\omega_J^2/\gamma\omega_c,$$
$$\tan\theta=(\omega^2-\omega_c^2)/\gamma\omega_c, \quad (30)$$

or alternatively,

$$\omega/\omega_c=[1+(\gamma/\omega_c)\tan\theta]^{1/2}. \quad (31)$$

Thus Γ is a dimensionless measure of the strength of the coupling of the current to the resonance, while $\tan\theta$ is a measure of the departure of the dc bias from a multiple of the resonance frequency. The phase shift φ can be eliminated from Eq. (28) to yield the implicit algebraic equation for Z,

$$Z/\Gamma=|[J_{m-1}(Z)]^2-[J_{m+1}(Z)]^2|\{[J_{m-1}(Z)-J_{m+1}(Z)]^2+[J_{m-1}(Z)+J_{m+1}(Z)]^2\tan^2\theta\}^{-1/2}. \quad (32)$$

Furthermore, if Eq. (28) is satisfied, then the dc component of the Josephson current can be rewritten in the very simple form

$$\langle\mathfrak{J}(t)\rangle_t/j_J=(2\pi)^{-1}\int_0^{2\pi} d(\omega t)\cos[m\omega t+Z\cos(\omega t+\varphi)]$$
$$=Z^2/2m\Gamma. \quad (33)$$

We have solved Eq. (32) graphically, by plotting the left- and right-hand sides of the equation as functions of Z and reading off the points of intersection. This has been carried out for the three values $m=1$, 2, and 3, assuming a resonator $Q=7.5$ to conform to our analog work. The results for the dc current are shown in Figs. 11–15. Figures 11, 13, and 15 show the dc current as a function of coupling strength Γ for various values of $\tan\theta$, while Figs. 12 and 14 show the current as a function of $(\omega/\omega_c)-1$ for various Γ, the latter form of plot being closest to the analog-generated dc characteristics presented in Sec. IVB.

The case of $m=1$ has already been analyzed in Ref. 23 and in fact Fig. 11 is taken directly from that paper. (With the exception that a factor-of-2 error in the ordinate has been corrected here.) The rearrangement of the results into the "line-shape" plot of Fig. 12 has not been carried out before, however. The fact that the line shapes agree qualitatively and semiquantitatively (discrepancies are of order 10–15%) indicate that our approximation (27) is a satisfactory one.

Figures 13 and 14 give the same plots for $m=2$. Here there is no dc current unless Γ is greater than a finite value and the dc current rises steeply for Γ increased slightly above threshold, two features also found in the analog solutions. The line shapes are again similar to those seen in the analog solutions.

Figure 15 shows the current versus Γ plot for $m=3$.

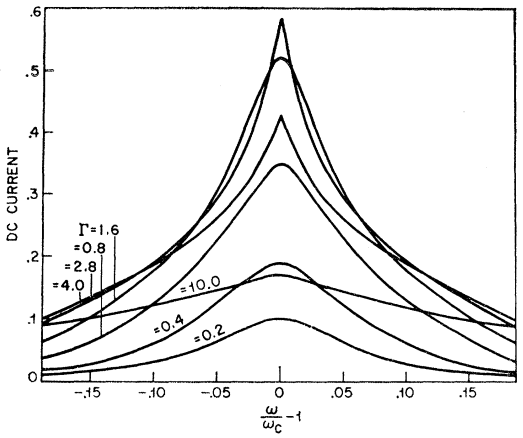

FIG. 12. The dc component of current versus normalized dc bias, for various Γ; $m=1$.

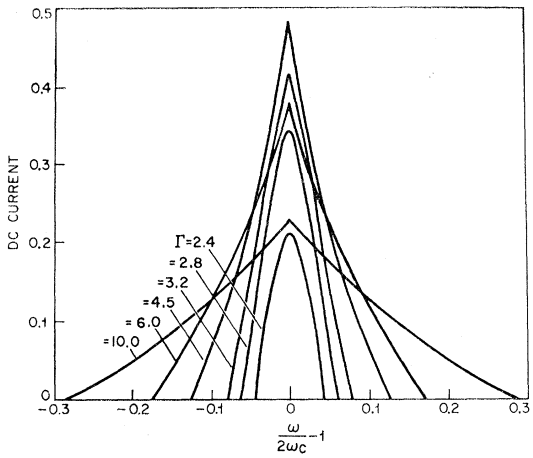

FIG. 14. The dc component of current versus normalized dc bias, for various Γ; $m=2$.

Not only is there a threshold in Γ below which the dc current is zero, but now the current jumps discontinuously to a nonzero value as Γ is increased through the threshold! Furthermore, the solutions are double valued for fixed Γ and θ; a serious instability would take place at such an operating point as the system switched randomly between the two degenerate solutions. This behavior was observed in the analog simulation but it could not be illustrated in a figure. Examination of Eq. (32) shows that features similar to these for $m=3$ also occur for all larger values of m.

Although it would be extremely interesting to observe these effects experimentally, the real situation presents complications. For any actual cavity there is likely to be another resonance (with twice as many spatial nodes) at nearly twice the frequency of a given resonance. This second resonance, not included in our prototype equations, would substantially interfere with the second harmonic of the given resonance. However, it does not seem out of the question to design an experiment which circumvents this difficulty.

The approximation we have used here is also applicable to the case of an added rf voltage drive, as in Fig. 8. The absorption and emission lines there can all be understood both as to sign and magnitude by an analysis generalizing only slightly that given above. If the dc bias voltage is at $\Omega_{dc}=m\omega+n\omega_{rf}$, where again $\omega\approx\omega_c$, the result is that Eq. (32) is modified only by the change

$$\Gamma\rightarrow\Gamma\mid J_n(\Omega_{rf}/\omega_{rf})\mid, \tag{34}$$

while Eq. (33) for the dc current remains unmodified. Thus the rf modulation only alters the effective coupling strength of the ac currents with the resonance. Equation (33) shows that the dc current is proportional to the sign of m, and hence that all lines with negative m are emissive, as is observed in Fig. 8. On the other hand, the dispersive lines of Fig. 8, involving halving of the rf frequency, are not understood so easily, since the electromagnetic cavity is not driven on resonance and does not contain predominantly a single frequency component.

In addition to the dc component of the Josephson current given by Eq. (33), we can also easily work out the frequency component at the rf frequency, a quantity appropriate to the experiment of Silver and Zimmerman.[21] Although we do not quote the final formula, this component turns out to be essentially

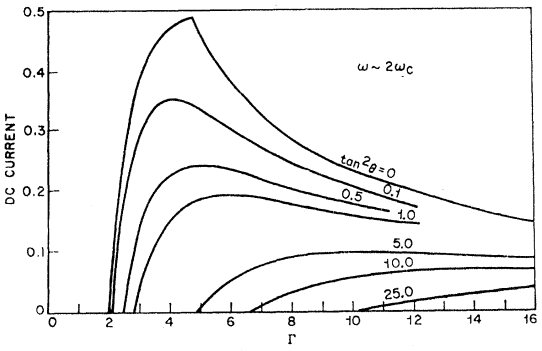

FIG. 13. The dc component of current versus Γ, for various $\tan\theta$; $m=2$.

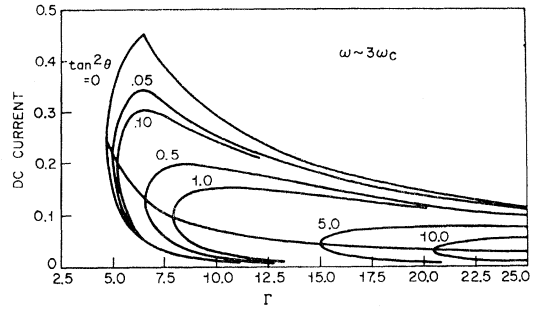

FIG. 15. The dc component of current versus Γ, for various $\tan\theta$; $m=3$. The curves are double valued, and an added line connects the points of infinite slope.

the dc bias voltage derivative of the dc component, a result already understood by those authors.

VI. SUMMARY

We have demonstrated that equations characterizing a Josephson junction coupled to a resonant cavity and driven by an applied rf field are amenable to solution on an analog computer. The computer results have been contrasted with those of pertinent experiments and have indicated where further experimentation is desirable. The results have demonstrated a number of the nonlinear and parametric effects possible in the Josephson effect. With the approximation that only the resonance frequency can assume appreciable amplitude in the cavity—an approximation shown to be suitable by the analog work—analytical expressions have been derived for line shapes in a number of cases of interest. Finally we should note that the cases calculated here by no means exhaust those to which the analog technique can be applied.

ACKNOWLEDGMENTS

It is a pleasure to thank Paul D. Stark for his help in making the analog computer available to us and instructing us in operation. We have benefited from encouraging conversations with Dean E. McCumber.

PHYSICAL REVIEW VOLUME 164, NUMBER 2 10 DECEMBER 1967

Flux-Flow Resistivity in a Superconducting Disk

M. P. SHAW AND P. R. SOLOMON
United Aircraft Research Laboratories, East Hartford, Connecticut
(Received 21 June 1967)

The flux-flow resistivity of a type-II superconductor in the mixed state was studied by passing a symmetric radial current through a superconducting disk. The experiment verified that current-induced flux flow does not require a gradient in the density of flux lines in the direction of flux motion.

THE motion of quantized magnetic flux lines (vortices) and associated flux-flow resistivity in type-II superconductors has been studied in detail during the past few years. In most experiments, current was passed down the length of a thin superconducting strip in a magnetic field applied perpendicular to its surface.[1] Current-induced magnetic fields gave rise to a gradient in the density of flux lines in the direction of flux motion. Since there was some confusion as to the role that this gradient plays in flux flow,[2] we looked for flux-flow resistivity in a geometry in which there are no flux-line gradients in the direction of flux motion. This was accomplished by passing a symmetric radial current through a superconducting disk in a homogeneous magnetic field. When sufficient current was passed through the disk a radial potential gradient was observed. Assuming that the potential gradient arises from flux motion, the experiment proves that a gradient in the density of flux lines in the direction of motion is not required for flux flow.

The experimental arrangement is shown in Fig. 1. A superconducting disk had current leads attached at the center and at the perimeter so that current flowed radially. A perpendicular magnetic field was applied. The field lines shown in Fig. 1 represent the sum of the externally applied field and the field produced by the current in the sample. If flux lines flow in this geometry, symmetry requires that they describe circles concentric with the disk since steady-state motion could not be sustained if flux lines move radially. Leads were attached for measuring the potential gradient which should be observable along the radius.

Figure 2 shows the arrangement used to ensure cylindrical symmetry of the sample and leads. A current lead is connected to the center of a heavy copper disc which is soldered to the end of a heavy copper pipe about 6 in. long. The other end of the pipe is attached to the perimeter of the disk. An indium gasket squashed between the disk and the copper pipe ensures good electrical contact. The other current lead, which passes through a hole drilled in the copper disk, is screw clamped to the center of the sample. If the disk and copper pipe are homogeneous, this geometry ensures a symmetric current in the superconductor and hence circular flux orbits. If there are inhomogeneities in the disk, the flux orbits would still remain roughly

[1] See, for example: Y. B. Kim, C. F. Hempstead, and A. R. Strnad, Phys. Rev. **139A**, 1163 (1965); J. Volger, F. A. Staas, and A. G. van Vijfeijken, Phys. Letters **9**, 303 (1964); W. F. Druyvesteyn and J. Volger, Philips Res. Repts. **19**, 359 (1964); P. H. Borcherds, C. E. Gough, W. F. Vinen, and A. C. Warren, Phil. Mag. **10**, 349 (1964). For experimental verification of the flux flow hypothesis, see: I. Giaever, Phys. Rev. Letters **15**, 825 (1965); P. R. Solomon, *ibid.* **16**, 50 (1966).

[2] The force on a vortex in a current carrying strip derived by Y. B. Kim *et al.* (Ref. 1) is directly proportional to the flux-line gradient. M. Tinkham [Phys. Rev. Letters **13**, 804 (1964)], however, pointed out that for a flat strip the driving force comes from the tension in the bent field lines and not from a flux-line gradient. A recent calculation of the force on a vortex by J. E. Evetts and A. M. Campbell [in *Proceedings of the Tenth International Conference on Low-Temperature Physics, Moscow, 1966* (Proizvodstrenno-Izdatal'skii Kombinat VINITI, Moscow, USSR, 1967)] is in agreement with Tinkham's interpretation.